Dalton Transactions

ROYAL SOCIETY OF CHEMISTRY

PAPER

View Article Online
View Journal | View Issue

Cite this: *Dalton Trans.*, 2024, **53**, 9995

Aldehyde-containing clays: a sustainable approach against the olive tree pest, *Bactrocera oleae*†

Stefano Econdi,[a,b] Chiara Bisio, *[a,c] Fabio Carniato, [c] Stefano Marchesi, [c] Geo Paul, [c] Elisabetta Gargani,[d] Ilaria Cutino,[d] Alessandro Caselli [b] and Matteo Guidotti *[a]

A set of organic/inorganic layered materials was obtained by functionalizing a montmorillonite-containing bentonite natural clay with linear aliphatic C_6 or C_7 aldehydes through a cost-effective and technologically simple incipient-wetness deposition method. The solids were investigated by means of a multi-technique approach (X-ray powder diffraction, XRPD, scanning electron microscopy, SEM, Fourier-transform infrared spectroscopy, FT-IR, thermogravimetric analysis, TGA, elemental analysis and solid-state nuclear magnetic resonance, ssNMR) to clarify the nature of the deposited organic species and the mode of interaction between the aldehyde and the clay. Since both natural clays and short-chain linear aldehydes find application as alternative strategies in the control of the olive fruit fly, *Bactrocera oleae*, the hybrid layered materials were tested under real-life conditions and their insect-inhibiting capability was evaluated in open-field trials on olive tree orchards in Tuscany, Central Italy. Specific tests were conducted to evaluate the resistance of the solids to weathering and their capability to provide a constant and long-lasting release of the bioactive ingredient. Aldehyde-containing bentonite clays have shown promising performance in controlling *B. oleae* infestation (with up to 86–95% reduction of affected olive fruits) in open-field trials across two years in two locations with different pedological and meteo-climatic characteristics.

Received 8th March 2024,
Accepted 20th May 2024

DOI: 10.1039/d4dt00705k

rsc.li/dalton

Introduction

Olea europaea, the common olive tree, is an evergreen fruit tree known for its exceptionally long lifespan which, under favourable conditions, can live for up to a thousand years. Despite its origin in the Near East, the primary cultivation area is concentrated in the Mediterranean Basin, contributing to 97% of global olive oil production.[1] The worldwide significance of the olive oil market has prompted a heightened focus on sustainable methods to protect olive trees from pests and phytophagous organisms, addressing both environmental and economic concerns. A major threat to olive crops on a global scale,[2] particularly in the Mediterranean region, is the olive fruit fly, *Bactrocera oleae* (Rossi) (Diptera, Tephritidae). This widely distributed species is recognized for causing substantial damage, leading to significant yield losses and diminished quality of olives and their derived products.[3,4] The economic impact is substantial, with an estimated annual reduction of 15% in world production attributable to *B. oleae*. As a result, efforts are underway to develop sustainable and effective strategies to mitigate the impact of this pest on olive cultivation. The use of synthetic insecticides[5] based on organophosphate, pyrethroid or neonicotinoid compounds represents the strategies mostly followed in the fight against this pest. In particular, dimethoate (*O*,*O*-dimethyl *S*-methylcarbamoylmethyl phosphorodithioate), phosmet (a related phthalimide-derived organophosphate insecticide), deltamethrin, lambda-cyhalothrin, alpha-cypermethrin[6] or acetamiprid are active ingredients that are currently widely used in the control of the olive fly. They feature low costs, high efficacy against larvae and good persistence on the olives.[7] More recently, Spinosad,[8,9] an active substance of biotechnological origin, extracted from the metabolites of the soil bacterium *Saccharopolyspora spinosa*, with a broad-spectrum insecticidal activity, has also come into use (Fig. 1). All these active ingredients exert a neurotoxic activity on the insect, thus interfering with synaptic nerve impulse transmission, leading to the death of the organism they act upon.

Nevertheless, all these insecticides have also shown adverse effects on various non-target animals including mammals, birds, fish, bees and, in general, the environment.[10,11]

[a]*CNR-Istituto di Scienze e Tecnologie Chimiche "Giulio Natta", Via C. Golgi 19, Milan, Italy. E-mail: matteo.guidotti@cnr.it, chiara.bisio@uniupo.it*
[b]*Dipartimento di Chimica, Università degli Studi di Milano, Via C. Golgi 19, Milan, Italy*
[c]*Dipartimento di Scienze e Tecnologie Avanzate, Università del Piemonte Orientale, Via T. Michel, Alessandria, Italy*
[d]*Consiglio per la Ricerca in agricoltura e l'analisi dell'Economia Agraria CREA–Centro di ricerca Difesa e Certificazione DC, Florence, Italy*
† Electronic supplementary information (ESI) available. See DOI: https://doi.org/10.1039/d4dt00705k

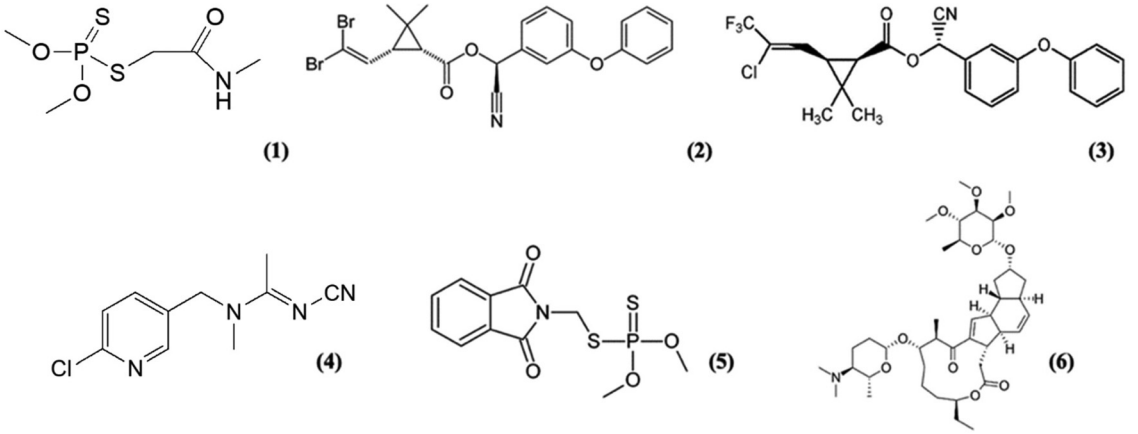

Fig. 1 Chemical structures of dimethoate (**1**), deltamethrin (**2**), lambda-cyhalothrin (**3**), acetamiprid (**4**), phosmet (**5**), and Spinosad (**6**).

Moreover, their extensive and long use has facilitated the development of insecticide resistance,[5,12–14] with a negative impact on beneficial entomofauna[15,16] and on the quality of olive oil.[17]

Therefore, the implementation of innovative and environmentally friendly control methods for this pest has gained significant attention. This interest has grown, especially after the years 2014, 2016, and 2019, when Southern European olive oil production suffered substantial losses in both quality and quantity.[18] Furthermore, the recent ban by the European Union on the use of dimethoate in olive crops starting in October 2020 has accelerated the need for alternative strategies.[19] These strategies increasingly emphasize the integration of various control methods that meet four main criteria: toxicological safety, environmental selectivity, pest control efficiency and economic sustainability. To prevent or mitigate the effects of fruit fly infestation, various inorganic solids can be applied to olive trees. Many of these systems meet the stringent requirements necessary for use in organic agriculture. Phyllosilicate clays and zeolites of natural origin have often shown interesting features in the protection of crops from pests and diseases.[20–24] This is attributed to their negligible toxicological impact, environmental compatibility and remarkable physico-chemical characteristics, in terms of cation-exchange capability and sorption properties. Finely ground mineral clays are indeed able to form a homogeneous particle film on plant leaves and tissues, hence acting as a viable strategy for controlling the infestation of parasitic species.[20–22] Analogously, zeolites can be successfully used in agriculture and find application in the reduction of heat stress and sunburn for crops, enhancement of photosynthetic processes and, especially, for their fungicidal and insecticidal properties.[25] From the perspective of the most common mineral species used for these purposes, two solids are mainly reported: montmorillonite, with the average composition $(Na,Ca)_{0.3}(Al,Mg)_2Si_4O_{10}(OH)_2{\cdot}n(H_2O)$, that is the main phyllosilicate clay in the natural commercial solid called bentonite, and clinoptilolite, that is a natural-origin zeolite having the minimum formula $(Ca,Na,K)_{2-3}Al_3(Al,Si)_2Si_{13}O_{36}{\cdot}12(H_2O)$, with a two-dimensional channel system (parallel to *a* and *c* axes) with openings in the range of 0.40–0.72 nm.[26] Both montmorillonite clay and clinoptilolite zeolite can readily act as adsorbents and ion exchangers.

Considering these properties, clays and zeolites have successfully found application in the protection of olive crops from olive fly as alternatives to conventional agrochemicals. They feature an indirect repellant action against *B. oleae*, as the inorganic material does not kill the parasite but, rather, negatively affects the recognition of the olive tree and fruit by the adult insect. In fact, when the plant surface is treated with a thin layer of solid, the visual, tactile and olfactive signals by which the fly can recognize the optimal location for egg deposition are masked or scrabbled and this leads to a disorienting action for the insect. Micronized zeolites or clays, in fact, create uniform films, which do not interfere with the metabolic lifecycle of plants but, in contrast, enhance their resistance to external pests and disease.[25–27] In addition, these solids, as adsorbing materials, are able to capture water molecules from the surface of leaves and fruits (drying effect), hindering the growth of fungi, larvae and other undesired parasitic species.[25]

Moreover, such a covering layer helps in protecting the plant from adult insects and other phytophagous arthropods, since the colouring and the microscopic surface structure of leaves and fruits are altered.[28,29] Then, the high adsorption capability of zeolites and clays makes them ideal materials for the targeted and controlled release of agrochemicals, semiochemicals and vegetable extracts useful in the protection of crops from pests. Agrochemicals can be deposited, inserted and/or chemisorbed on or in the pore network of zeolitic solids and rock powder or within the interlayer spaces of phyllosilicate clays, thus reducing the amount of active ingredients with a neat benefit in terms of environmental impact, frequency of treatments and amounts of chemicals used.[30,31]

In line with our ongoing research on aluminosilicate minerals as host plant masking solids,[32] these previous attempts

prompted us to design a novel class of composite oxidic materials capable of hosting an organic bioactive compound that can effectively disrupt the host-plant selection process of *B. oleae* adults, featuring a targeted, constant and mild release of the active species for a long-term treatment of the olive fruits. Several studies have demonstrated that medium-chain linear aliphatic aldehydes, specifically *n*-hexanal, *n*-heptanal, (*E*)-hex-2-enal and (*E*)-hept-2-enal, exhibit clear repellent and/or signalling activity against pests and parasitic organisms affecting crops.[33] In particular, these C_7 and C_6 aldehydes are effective semiochemicals and interfering agents against the olive fly, *Bactrocera oleae*, and are increasingly being applied for the protection of olive crops.[34–37] This includes their deposition and immobilization within lamellar solids in benchmark supports, such as synthetic saponite clays.[38]

The present study aims at designing and preparing a composite organic/inorganic (oxidic) layered material capable of accommodating a bioactive compound that is active in disrupting the host-plant selection process of *B. oleae* adults featuring a targeted, smooth and constant release of the bioactive species over time for a long-term treatment of the olive fruits. To this aim, a series of solids inducing an interference activity on the infestations of *B. oleae* have been prepared. The materials are based on an inorganic support, namely a bentonite clay (mainly composed of montmorillonite) of natural origin. The solids were used either in their native state or after the deposition of a bioactive principle based on organic compounds. The solids were fully characterized by a multi-technique approach (XRPD, SEM, FT-IR, TGA, CHN, elemental metal analysis and solid-state NMR) in order to understand the specific interaction between the aldehyde and the clay and to evaluate the release capability and the stability of the organic species in the materials under ambient conditions.

Finally, the solids were tested under real-life conditions and their insect-inhibiting capability was evaluated in open-field trials on olive tree orchards in Tuscany, Central Italy.

Experimental details

Materials

Two commercial samples of solid supports of mineral origin were selected:

• *Bentonite Gl obalfeed AR* (Ben; 50 kg batch no. 3101204) is a montmorillonite-containing natural mineral clay, kindly obtained from Laviosa Chimica Mineraria SpA, Livorno, Italy. Its elemental composition, expressed as % m/m, is: Na_2O (0.40%), MgO (2.28%), Al_2O_3 (14.18%), SiO_2 (72.32%), P_2O_5 (0.03%), K_2O (1.87%), CaO (0.91%), TiO_2 (0.26%), MnO (0.03%) and Fe_2O_3 (2.33%). The specific surface area of the Ben sample is 114 $m^2\ g^{-1}$, calculated from N_2 physisorption analyses at 77 K using the Brunauer–Emmett–Teller (BET) model. When Ben was used in its pristine state, it was pretreated as follows: an aliquot of 240 g of Ben was dried in an oven at 110 °C for 3 h and then cooled down for 30 min under anhydrous conditions. Aldehyde-containing solids were prepared by an incipient wetness approach. Linear saturated or unsaturated aldehydes were used, namely: *n*-hexanal (C6AN; Sigma Aldrich, ≥97%), *n*-heptanal (C7AN; Sigma Aldrich, ≥95%), (*E*)-hex-2-enal (C6EN; Tokyo Chemical Industry Ltd, ≥97%), (*E*)-hept-2-enal (C7EN; TCI, ≥95%). The main physical properties (boiling point, vapour pressure and water solubility) of the organic compounds used in this work are summarised in Table S1.† The support material Ben, after being pretreated, was placed in contact with a 150 mL solution of the desired aldehyde (15 mL or 13 mL for C7AN or C7EN and for C6AN or C6EN, respectively) in petroleum ether 40/60 (Sigma Aldrich). The solution was gently poured onto the clay and the impregnated solid was thoroughly mixed. It was then left to dry under a fume cupboard for at least 14 h to allow the complete evaporation of all the impregnation solution. The final solid was stored under anhydrous conditions. Five materials were obtained accordingly: Ben (native state), BenC6AN (Ben + *n*-hexanal), BenC7AN (Ben + *n*-heptanal), BenC6EN (Ben + (*E*)-hex-2-enal) and BenC7EN (Ben + (*E*)-hept-2-enal).

• *Zeolite clinoptinolite* (Zeo, batch: 014/2018) is a natural mineral zeolite, kindly obtained from Biohelp Your Planet Srl (Tarquinia, Italy), used in its native state (Zeo) as a reference material in open-field trials. Its elemental composition, expressed as % m m^{-1}, is: Na_2O (0.1–0.5%), MgO (0.9–1.2%), Al_2O_3 (10–12%), SiO_2 (62–65%), P_2O_5 (0.02–0.05%), K_2O (2.5–3.8%), CaO (2.4–3.7%), Cr_2O_3 (0–0.01%), MnO (0–0.08%) and Fe_2O_3 (0.7–1.9%).

Characterization

Elemental C,H,N analysis was performed on the materials containing organic compounds and the pristine materials to determine, through the difference in carbon content, the quantity of organic compounds added during the preparation steps. The analysis was carried out on a PerkinElmer model 2400 series II instrument and conducted under transistor-grade extra-pure oxygen (SIAD; residual N_2 < 50 ppm_{vol}) with helium (SIAD, 5.5 purity) as the carrier gas.

Absorbance FT-IR spectra were recorded using a FT-IR FTS-60 (Bio-Rad) spectrophotometer with a liquid nitrogen-cooled MCT (mercury telluride and cadmium) detector. Variable-temperature experiments were carried out on a Bruker Equinox 55 spectrometer in the range 4000–400 cm^{-1} with a resolution of 4 cm^{-1} using a dedicated apparatus and all thermal treatments (from 30 to 500 °C) were performed *in situ*. Infrared spectra of pure liquid aldehydes were collected at room temperature by using a cell for liquid samples.

Thermogravimetric analysis was carried out with a TGA 7HT (PerkinElmer) instrument connected to a TAC 7/DX PerkinElmer controller. The temperature program covered the range from 50 °C to 950 °C (with an increase of 3 °C min^{-1}), using extra-pure air as the analysis gas and nitrogen as the purge gas.

X-ray powder (XRPD) diffractograms were collected on unoriented ground powders with a ThermoARL X'TRA-048 powder diffractometer (Thermo Fisher Scientific, Waltham, MA, USA) with Cu-$K_{\alpha 1}$ (λ = 1.54062 Å) monochromatic radiation.

Diffractograms were recorded at room temperature (RT) in the 5°–80° 2θ range with a step size of 0.02° and a rate of 1.0° min^{-1}. The X-ray profiles at low angles (2–8° and 3–10° 2θ) were collected with narrower slits and at a rate of 0.25° min^{-1}.

Solid-state NMR (ssNMR) spectra were acquired on a Bruker Avance III 500 spectrometer equipped with a wide bore 11.74 T magnet and a 4 mm triple resonance probe. Powdered samples were packed on a zirconia rotor and spun at a magic angle spinning (MAS) rate of 10–15 kHz at 298 K. 1D experiments such as ^{1}H MAS and ECHO MAS NMR were conducted using a radio-frequency field of 100 kHz. The relaxation delay d_1 between accumulations was 5 s. A rotor-synchronized spin-echo sequence was applied to record the ^{1}H ECHO MAS NMR spectra with a delay time τ of 2010 ms. All chemical shifts were reported on the δ scale and externally referenced to tetramethylsilane at 0 ppm.

Scanning electron microscopy (SEM) images were collected on a Philips/FEI Quanta 200 Environmental SEM (ESEM) using a tungsten filament as an electron source (200 keV) and a back-scattering detector operating at low vacuum. A conductive coating of gold (sputtering thickness of 10 nm) by low-pressure plasma was deposited on samples, previously placed on carbon grids, to avoid the presence of electronically charged insulating particles under the electron beam.

Weathering tests

In the tests to evaluate the robustness of aldehydes to leaching and weathering from the materials, the solids were extracted not only with ultrapure Milli-Q water, but also with acidified water (by diluted acetic acid) to simulate the presence of natural rainwater at its typical pH (pH ~5). The aldehyde-containing material, 1.00 g, was weighed and dispersed into 10.0 mL of water. After 30 min, the suspension was filtered using a funnel with filter paper. The solid phase was used for C, H, N analysis, while 1.00 mL was extracted from the liquid phase with 5.00 mL of dichloromethane, adding 5.0 μL of *n*-decane (Aldrich) as an internal standard. The GC-FID analysis of the organic phase was carried out with an Agilent 6890 series instrument (Agilent 19091J-413–30 m × 0.320 mm, He carrier gas, and at a pressure of 144.79 kPa) with the following program: $T_{initial}$ 60 °C, $t_{initial}$ 20 s – $Rate_1$ 10 °C min^{-1}, T_{final1} 90 °C, t_{final1} 0 min – $Rate_2$ 50 °C min^{-1}, T_{final2} 195 °C, t_{final2} 1 min. Retention times (min) are as follows: t_r hexanal = 1.340; t_r heptanal = 1.895; t_r hexenal = 1.595; t_r heptenal = 2.317; t_r *n*-decane = 2.748.

Field tests

Prior to use in open-field trials, each batch of the above-mentioned solids (240 g) was dispersed in 1.00 L of ultrapure deionized water (MilliQ water, 10^{-10} S cm^{-1}) by mechanical stirring for 15 min and then the suspension was transferred in a 1.5 L plastic food-grade PET bottle. Each PET bottle contained one dose of solid suitable for the treatment of 3 olive trees. In order to evaluate the performance of the most promising solids, field trials were performed in the years 2018 and 2019. In the first year, 2018, the tests were conducted in traditional olive groves located in Tuscany in one olive plant orchard (24 trees) at Podere Forte farm in Castiglione d'Orcia, Siena province (geographical coordinates: 43.00671° N; 11.59636° E) on Moraiolo and Frantoio olive cultivars. In the second year, 2019, field trials were performed in an olive plant orchard (24 trees) at Marchesi Mazzei farm in Fonterutoli, Siena (geographical coordinates: 43.43577° N; 11.30643° E) specifically on Moraiolo olive trees. The materials tested in 2018 were respectively a natural montmorillonite-based clay (Ben), a natural clinoptinolite-based zeolite (Zeo), two bentonite clays functionalized with aliphatic aldehydes (BenC6AN and BenC7AN), a commercial product chosen by the farmer (Fertiram™) and a control plot (water treatment). In 2019, the natural montmorillonite-based clay (Ben), the natural clinoptinolite-based zeolite (Zeo), four products with bentonite and aliphatic aldehydes, either saturated or monounsaturated (BenC6AN, BenC7AN, BenC6EN, and BenC7EN) and a control solution (drinkable water from the local water supply system) were tested. The solid-in-water fine suspension of the products (3.1 wt% suspension of the solid in drinkable tap water) was spread onto the crop trees by means of a backpack sprayer at normal volume. During the trials, on each olive crop, three treatments (T1, T2, and T3) were carried out at normal volume from the mid of July to the mid of September. The average temperature values in the months of the application of the materials are summarized in Table S2† (ESI section). Each year, experimental plots were set up in the chosen olive crops, identifying the different thesis, whose repetitions were randomly distributed into the fields. In each plot, chromotropic and pheromone traps were positioned to monitor the presence of the *B. oleae* population. When the olive fruits have become susceptible to the olive fruit fly egg laying, 100 fruits per thesis were picked up and analysed under a stereomicroscope to check the presence of living or dead *B. oleae* preimaginal stages on the fruits. The tests on controls were performed before the experimental treatment and every 10 days after that. The effect of the treatments on *B. oleae* was evaluated by checking the total infestation on olive fruits, comparing the different thesis.

Results and discussion

Characterization of the solids

Commercial bentonite, Ben, a natural montmorillonite-containing mineral clay with a typical sheet-like or lamellar morphology, is constituted by tactoids of different sizes in the 3–5 μm range as observed by scanning electron microscopy (SEM) as shown in Fig. 2.

The structural features of bentonite before and after impregnation with the aldehydes were investigated by X-ray powder diffraction (XRPD). The pristine Ben sample shows the typical crystallographic reflexes of the montmorillonite phase,[39] which represents the main component in the X-ray pattern (Fig. 3A). No other relevant crystalline components were revealed by XRPD analysis. When the pristine Ben sample

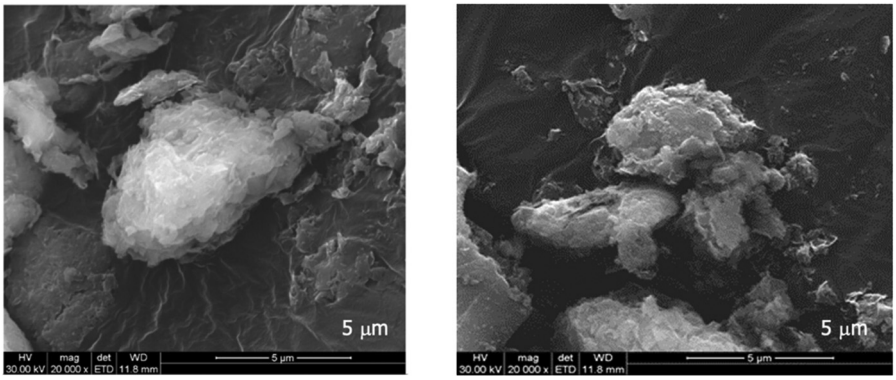

Fig. 2 SEM micrographs of the natural clay sample, Ben.

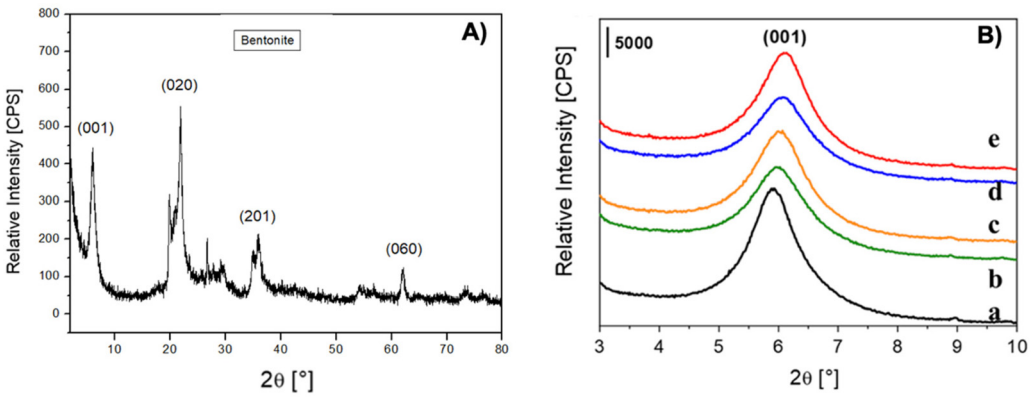

Fig. 3 (A) X-ray powder diffraction profiles of Ben; (B) diffractograms of bentonite samples before and after impregnation with the aldehydes, collected in the 3–10° 2θ range: Ben (a), BenC6AN (b), BenC6EN (c), BenC7AN (d) and BenC7EN (e).

was directly impregnated with the aldehydes, the intense and very well resolved (001) signal slightly shifted towards lower *d*-spacing values (Fig. 3B, b–d and Table 1), with a small broadening and reduction in intensity of the reflection in general.

This behaviour suggests that the impregnation of both saturated and unsaturated aliphatic aldehydes during the preparation steps does not lead to any evident expansion of the *d*-spacing between the TOT layers of the clay. Rather, since Ben can absorb up to 4.5 wt% of physisorbed water under open-air conditions (as from TGA analysis, see Fig. S4a†), the small, but non-negligible, decrease of $d_{(001)}$ spacing observed in the hybrid materials (Table 1) can be associated with the removal of water molecules during the thermal pretreatment before the impregnation step.

By elemental C,H,N analysis, the changes in carbon content and thus the organic fraction deposited onto the solids were determined.

The pristine bentonite clay, Ben, contains a minimal amount of carbon (0.17%), likely due to inorganic carbonate species, since the material is of mineral origin (Table 2). Upon aldehyde adsorption, there is a significant increase in carbon

Table 1 *d* spacing values of the (001) reflection for Ben and the four aldehyde-impregnated bentonite samples, derived from the diffractograms in Fig. 3

Sample	$d_{(001)}$ spacing [nm]
Ben	1.499
BenC6AN	1.475
BenC6EN	1.461
BenC7AN	1.452
BenC7EN	1.448

Table 2 Results (wt%) of the CHN analysis of inorganic–organic hybrid materials obtained starting from pristine clay Ben. A standard deviation of ±0.20% for C and ±0.40% for H and N is to be considered

Ben	BenC6AN	BenC7AN
C: 0.17%	C: 2.99%	C: 3.66%
H: 1.21%	H: 1.35%	H: 1.48%
N: 0.19%	N: 0.04%	N: 0.01%
Ben (treated with solvent)	**BenC6EN**	**BenC7EN**
C: 0.09%	C: 2.86%	C: 3.82%
H: 1.31%	H: 1.34%	H: 1.43%
N: 0.03%	N: 0.00%	N: 0.00%

content, which is clear evidence that the deposition of organic species was successful. The contribution to the carbon content by potential residues of petroleum ether solvent (used for aldehyde deposition) is negligible (as shown in the fourth entry of Table 2 (C: 0.09%), where the pristine bentonite was treated with petroleum ether alone in the absence of aldehydes). In this case, values of hydrogen content are not meaningful because the solid could not be dried in an oven due to the volatility of the aldehyde. Therefore, the presence of absorbed water from atmospheric moisture cannot be excluded or properly monitored.

The mass percentage of the deposited aldehyde in the materials was calculated taking into account the initial carbon present in the pristine bentonite. The calculation was iterated until convergence, adjusting the initial mass of the bentonite support by subtracting the calculated mass of the adsorbed aldehyde. Aldehyde contents were the following:

n-hexanal in BenC6AN = 3.93 wt%; *n*-heptanal in BenC7AN = 4.75 wt%; (*E*)-hex-2-enal in BenC6EN = 3.75 wt%; (*E*)-hept-2-enal in BenC7EN = 4.67 wt%

Weathering tests

When these clay-based materials are applied to the olive fruit and leaves, they adhere onto the surfaces of the vegetables thanks to the micronized form of these powders. However, exposure to atmospheric moisture and rainfalls might lead to the leaching and/or desorption of the aldehyde out of the clay carrier. To verify the stability of the aldehydes within the materials, leaching and weathering tests were carried out both in the presence of Milli-Q ultrapure water and by immersing the solid in acidified water for 30 min to simulate the exposure to heavy rainfalls with rainwater at its typical pH (pH ~5). *n*-Decane was used as an internal standard for quantification purposes. In none of the tests, from the GC-FID analysis, peaks at the retention times corresponding to the four aldehydes were detected in the organic phase used for the extraction from the aqueous weathering media (Fig. S1 and S2†). The aldehyde content after contact with both neutral and acidified water was thus below the detection limit, demonstrating a good degree of resistance to the weathering of the material.

The solids subjected to the weathering tests underwent elemental C,H,N analysis to determine the residual content of aldehyde species. Bentonite clays containing saturated aldehydes exhibit good resistance to leaching compared to the ones containing unsaturated aldehydes (Table 3) and 75% to 60% of hexanal and heptanal were still found in the solid at the end of the test. Conversely, in the clays containing unsaturated aldehydes, a significant decrease in carbon content was observed, with only 30% to 6% of the original hexenal or heptenal left on the solid. Since no detectable presence of aldehydes was revealed by GC-FID analysis in the aqueous phase, the bioactive species was likely displaced from the solid directly into vapour form without dissolving in the washout medium, with the solubility of these aldehydes in water being indeed scarce (*vs.* Table S1†).

Table 3 Elemental CHN analysis on the solids subjected to weathering tests. Column 1: materials before the test; column 2: materials after 30 min-contact with Milli-Q ultrapure water (W); column 3: materials after 30 min-contact with acidulated water at pH 5 (WH^+)

BenC6AN	BenC6AN (W)	BenC6AN (WH^+)
C: 2.64%	**C:** 1.99%	**C:** 1.54%
H: 1.49%	**H:** 1.43%	**H:** 1.38%
N: 0.04%	**N:** 0.03%	**N:** 0.01%
BenC7AN	BenC7AN (W)	BenC7AN (WH^+)
C: 3.66%	**C:** 2.38%	**C:** 2.43%
H: 1.48%	**H:** 1.45%	**H:** 1.33%
N: 0.00%	**N:** 0.07%	**N:** 0.08%
BenC6EN	BenC6EN (W)	BenC6EN (WH^+)
C: 2.86%	**C:** 0.19%	**C:** 0.30%
H: 1.34%	**H:** 1.43%	**H:** 1.18%
N: 0.00%	**N:** 0.00%	**N:** 0.04%
BenC7EN	BenC7EN (W)	BenC7EN (WH^+)
C: 3.82%	**C:** 1.16%	**C:** 1.03%
H: 1.43%	**H:** 1.27%	**H:** 1.22%
N: 0.00%	**N:** 0.00%	**N:** 0.00%

Weathering tests using simulated rainwater have underscored the fair robustness of the hybrid organic/inorganic layered solids, especially the ones containing saturated aldehydes, against weathering under harsh conditions, simulated by a full immersion in aqueous medium for 30 min.

Controlled release tests of the bioactive component

The controlled release of the bioactive principle over time was studied by simulating in the laboratory the climatic conditions of a typical summer season in Central Italy, where the open-field trials have been carried out. The aldehyde-containing clays were exposed to open air for 65 days at variable room temperature (ranging between 20 °C and 27 °C) and variable relative humidity (43%–88% RH) and then monitored through C,H,N analysis.

From the carbon content profile over time, in terms of controlled smooth release of the bioactive ingredient, the most promising type of material is the one containing saturated aldehydes, *i.e.* BenC6AN and BenC7AN (Fig. 4). Conversely, in line with the observations after weathering tests (see above), with unsaturated aldehydes, especially in BenC6EN, the carbon content of the organic ingredient fell below the reliable quantification limit for the instrument after *ca.* 4 weeks. For this reason, the C,H,N elemental analysis measurements was terminated on the 39th day for BenC6EN and BenC7EN. Such further observation suggests that a different mode of interaction between the aldehyde and the bentonite support takes place, moving from saturated aldehydes to unsaturated ones.

In Fig. S3,† the total weight of the solid for BenC6AN is constantly monitored and reported with the relative humidity of the day of the measurement (thus mimicking a real open-field exposure to summer weather). It is evident that the total

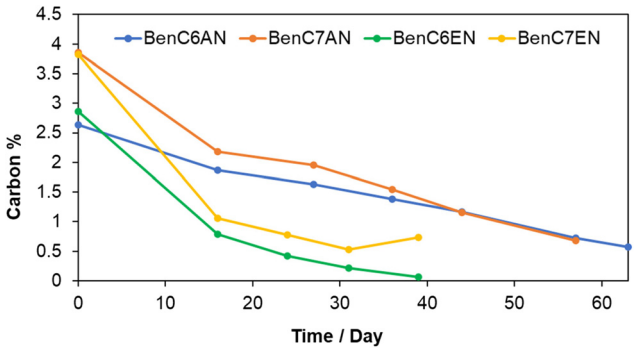

Fig. 4 Trend of the carbon content (wt%, by elemental C,H,N analysis) over time for BenC6AN (blue), BenC7AN (orange), BenC6EN (green) and BenC7EN (yellow). Experimental conditions: 65 days; temperature 20 °C–27 °C; relative humidity 43%–88%.

weight of the clay material is mainly governed by the amount of humidity taken or released, on a daily basis, under ambient conditions. The gradual loss of the bioactive aldehyde, conversely, is negligible under these conditions with respect to the oscillations of the overall weight.

From these observations, it can be concluded that the layered solids containing saturated aldehydes were more gently released over time compared to the ones containing unsaturated aldehydes. The saturated aldehyde-containing bentonite systems are therefore promising candidates to ensure a constant and long-lasting release of the bioactive ingredient into the surrounding atmosphere up to 60 days after deposition. Such behaviour is a critical feature when envisaging the use of these layered solids in open-field trials.

Solid-state NMR analysis

^{1}H MAS and ECHO ssNMR data (Fig. 5) provided direct information about the different proton species present in aldehyde-containing bentonite samples. In the ^{1}H MAS ssNMR spectrum of the pristine Ben sample (Fig. 5A, e), two peaks are present: a relatively narrow peak at around 4.5 ppm and a broader peak in the 1–8 ppm range. The former is due to interlayer water, while the latter is due to various hydroxyl moieties from the inorganic layers.[38,40] After the aldehydes are deposited onto the bentonite clay samples, all spectra exhibit peaks due to water along with narrower resonances associated with aldehydes (Fig. 5A, a–d).[38,41,42] The major signals observed are unambiguously assigned to the aliphatic protons (0.8–2.5 ppm) of the aldehydes. Narrow peaks (5.7 and 6.9 ppm) associated with the protons bound to unsaturated carbons are also found, especially in the spectra of BenC6EN (Fig. 5A, c). However, only a very weak broad peak is detected in BenC7EN, testifying that (*E*)-hept-2-enal is present in a limited amount in the sample. Well-resolved ^{1}H ECHO ssNMR spectra are obtained with a rotor-synchronized spin-echo sequence and are shown in Fig. 5B. Sharp resonances associated with the aldehyde species indicate that significant amounts of these molecules are mobile and experience weaker interactions with the host surfaces.[43] However, aldehydes may also interact strongly with host hydroxyls as shown by the broad peaks in the ^{1}H MAS ssNMR spectra.[44] Therefore, we can affirm that the solid-state NMR spectroscopic analysis confirmed the presence of aldehydes within the solid, which did not undergo any direct chemical transformation into different side products.

TGA analysis

By thermogravimetric analysis it was possible to monitor the loss of mass with the increase of temperature. In the TGA profile of bentonite (Fig. 6), the most significant mass loss occurs in the initial part of the curve (up to 130 °C *ca.*), primarily due to the evaporation of loosely-bound physisorbed water. Then, further mass is lost beyond 130 °C, but at a slower rate,

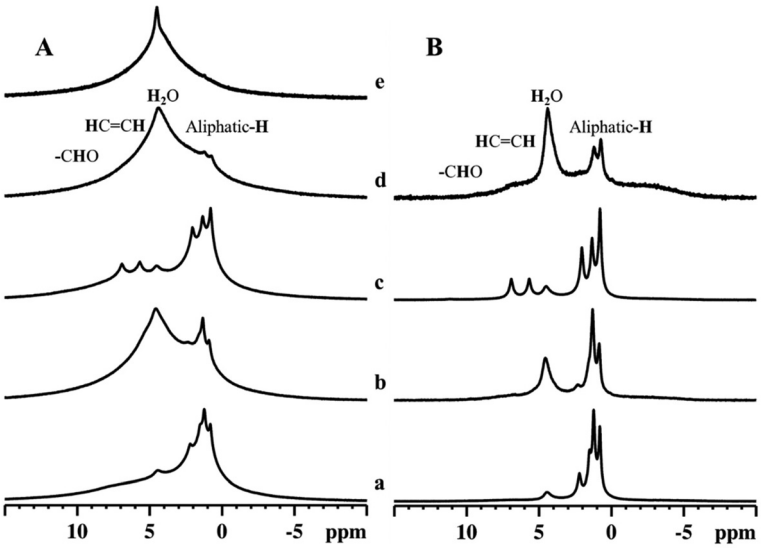

Fig. 5 ^{1}H MAS (A) and ECHO (B) NMR spectra of BenC6AN (a), BenC7AN (b), BenC6EN (c), BenC7EN (d) and Ben (e) samples.

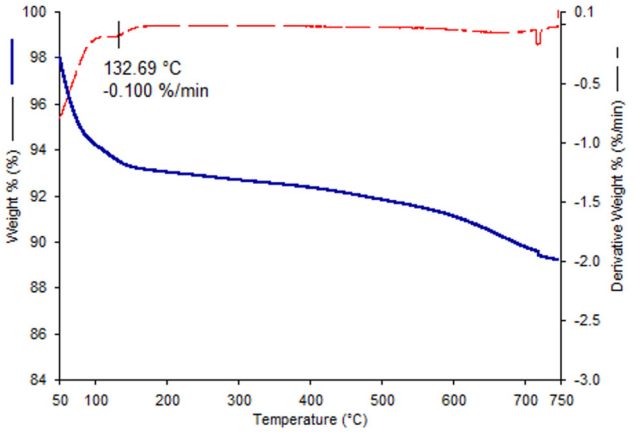

Fig. 6 TGA (blue curve) and DTG (red curve) profiles of the pristine Ben material. Analysis conditions: 50–750 °C range; 3 °C min^{-1}; extra-pure air.

attributed to the removal of the hydration water of the interlayer cations.[45] In order to calculate the mass loss, excluding the contribution of physisorbed water, in this study, the boundary between these two phenomena was defined at 120 °C. At higher temperatures, over 600 °C, a further significant decrease is noted due to the dehydroxylation of framework OH groups and a gradual collapse of the layered structure of the montmorillonite of the bentonite.

An analogous behaviour is recorded for the aldehyde-containing materials (BenC6AN; Fig. 7A and BenC7AN; Fig. 7B). Compared to pristine bentonite, however, the weight loss between 120 °C and 520 °C *ca.* is due to the evaporation/degradation of the aldehyde. Actually, aldehyde-bentonite composites contain a lower amount of water, as they are carefully dried at 110 °C prior to the impregnation of aldehydes. Because of the deposited organic species, their surface becomes more hydrophobic than the pristine Ben solid. A remarkably low amount of physisorbed water is therefore observed in the initial part of the TGA profile between 50 °C and 130 °C in Fig. 7. The different degradation temperatures of the aldehyde are attributed to its different locations within the material. The weight loss at lower temperatures is likely due to the fraction of aldehyde loosely adsorbed mainly on the external surface of the bentonite. The second weight loss at higher temperatures (250–350 °C) is caused by the degradation of the intercalated aldehyde fraction, which is delayed under harsher conditions, thanks to the protective and thermal stability effect of the clay structure on the organic additive.[38,46] Eventually, structural collapse above 600 °C is always present (Fig. 7A and B). When computing the mass losses, the materials containing aldehydes exhibit a larger mass loss than the pristine Ben clay (Fig. S4†), expressed as:

$$\Delta m_{\mathrm{Ben}} = 4.57\ \mathrm{wt\%};\ \Delta m_{\mathrm{BenC6AN}} = 8.31\ \mathrm{wt\%};\ \Delta m_{\mathrm{BenC7AN}} = 9.00\ \mathrm{wt\%}$$

and when subtracting the mass loss merely due to the clay support itself, the mass loss due to the presence of the aldehydes alone is expressed as follows:

$$\Delta_{\mathrm{BenC6AN}} = 3.74\ \mathrm{wt\%};\ \Delta m_{\mathrm{BenC7AN}} = 4.43\ \mathrm{wt\%}.$$

Interestingly, these data closely match the percentages of organic compound contents obtained from elemental C,H,N analysis.

FT-IR analysis

The presence of organic compounds on the bentonite materials and the type of interaction between the support and the deposited aldehyde were investigated by FT-IR spectroscopy. The pristine Ben solid showed characteristic absorption bands at around 3650 cm^{-1} and in the range 3500–3200 cm^{-1} due to the stretching of isolated and hydrogen-bonded OH groups, respectively, of the smectite sample. Moreover, bands between *ca.* 2100 and 1850 cm^{-1}, due to overtones and combination modes of the clay framework, and an absorption band at around 1640 cm^{-1}, assigned to absorbed water molecules, are also visible (Fig. 8).[47,48] In the spectra of

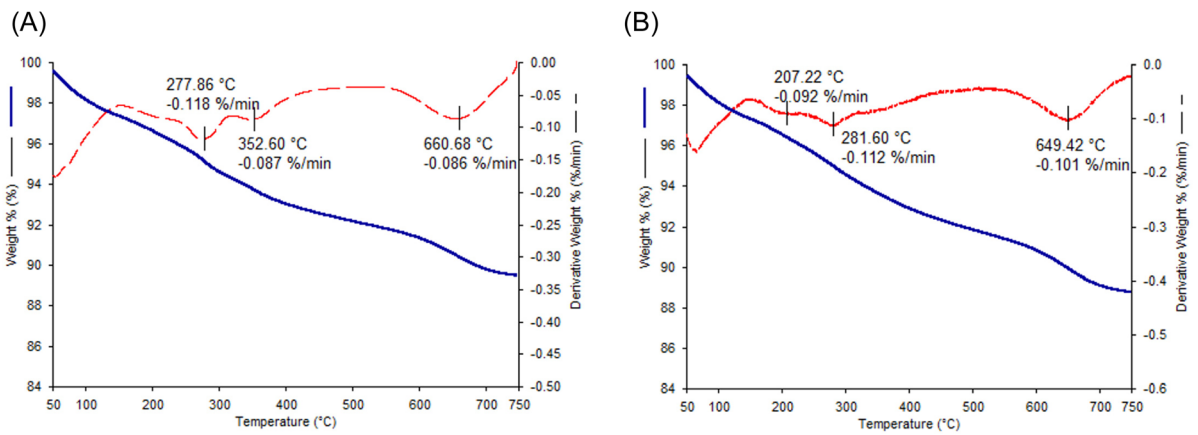

Fig. 7 TGA (solid blue curve) and DTG (dashed red curve) profiles of BenC6AN (A) and BenC7AN (B) materials. Analysis conditions: 50–750 °C range; 3 °C min^{-1}; extra-pure air.

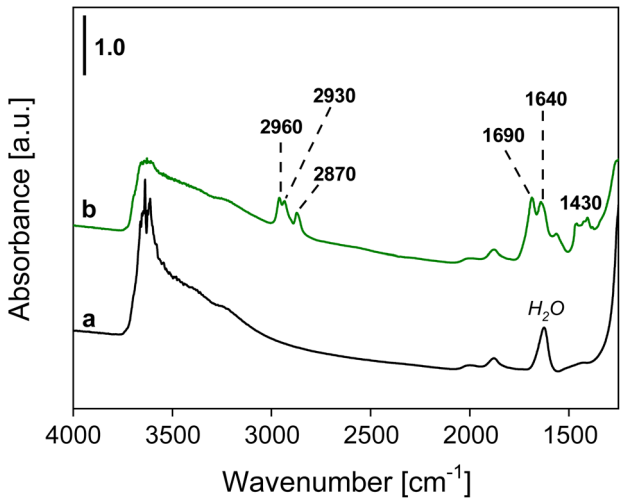

Fig. 8 FT-IR spectra in the 4000–1250 cm^{-1} region of Ben (a) and BenC6AN (b) clays.

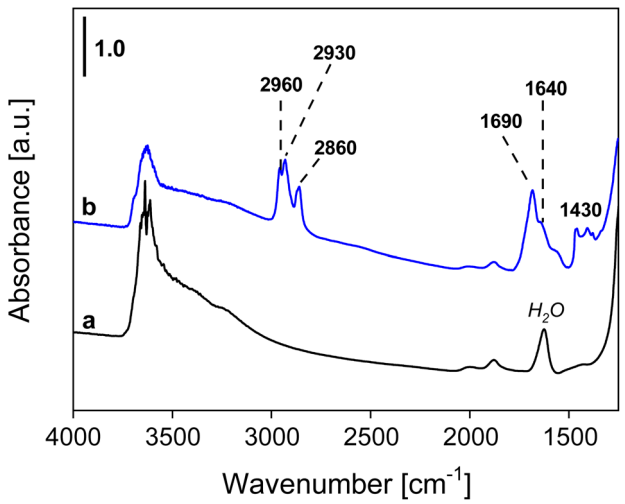

Fig. 9 FT-IR spectra in the 4000–1250 cm^{-1} region of Ben (a) and BenC7AN (b) clays.

the aldehyde-containing materials (Fig. 8 and 9), absorption bands at 2960, 2930, and 2870–2860 cm^{-1} corresponding to the symmetrical and asymmetrical stretching modes of C–H bonds within the aliphatic chains of the deposited aldehydes are present, while the band at 1430 cm^{-1} is associated with the bending modes of the –CH_3 group of the aldehydes.[49]

A band located at 1690 cm^{-1} or 1680 cm^{-1} for BenC6AN and BenC7AN, respectively, is visible in Fig. 8 and 9 and is attributed to the presence of the aldehydic carbonyl group. Interestingly, this band is shifted by 40 cm^{-1} and 50 cm^{-1} compared to the carbonyl stretching band of the free aldehydes in the liquid state (Fig. S5A†). This shift is therefore indicative of the weakening of the double bond, resulting in lower wavenumbers of $\nu_{C=O}$ absorption. Such observation suggests that the interaction between the aldehydes and the support is not a simple physisorption impregnation but, rather, a chemisorption interaction involving strong bonds between the δ^- oxygen of the aldehyde carbonyl group and the δ^+ Lewis acid sites on the clay, between the lamellae, at their edge and/or on their external surface (Fig. 10). In all these parts of the layered material, a relevant number of δ^+ interaction sites are indeed present and it is increased by the presence of a good fraction of transition metal heteroatoms (*e.g.* Ti, Mn, Fe; see the Experimental details section) dispersed throughout the natural clay.

By recording FT-IR spectra at variable temperatures (from 30 to 500 °C), a gradual elimination of adsorbed water from the clays was observed, with a clear diminution of the bands at 3500–3200 cm^{-1} and 1640 cm^{-1} (Fig. S6 and S7†). Accordingly, the bands attributed to the presence of the aldehyde decreased with increasing temperature. Nevertheless, a non-negligible presence of low-intensity bands due to the organic species (in the range 3000–2800 cm^{-1}) was detected even up to 500 °C. This is a further clue to the remarkable role of the montmorillonite structure in stabilizing a noteworthy fraction of the aldehyde within its interlayer spaces.[46,50]

This set of data confirms that organic aldehyde compounds are present on the bentonite-based materials (as shown by ssNMR too) and are bound to the clay support *via* dispersion and specific dipole–dipole interactions.[38] These specific interactions account for the robustness against weathering and leaching in aqueous solutions and the long-lasting smooth release of the bioactive ingredient into the surrounding atmosphere over time.

Open-field tests

In 2018, *B. oleae* infestation in the experimental areas in Siena province remained rather contained for the first part of the production season (late spring/early summer) and therefore no significant differences were highlighted after the first on-field treatments (T1 and T2). In September, the olive fruit fly population increased in number due to favourable climatic conditions. After the third treatment (T3), it is highlighted that the bentonite-based materials functionalized with aliphatic aldehydes (BenC6AN and BenC7AN) showed the best results compared to reference formulations, namely, the pristine clay (Ben), a natural clinoptilolite zeolite (Zeo) and the commercial treatment product (Fertiram™). In detail, BenC6AN and BenC7AN led to a percentage of total infestation less than 5% compared to over 23% of the control (water treatment) and 8% in the presence of Fertiram™ (Fig. 11). The trend displayed in the histogram suggests that there is a synergistic effect between the masking effect of Ben itself (*cf.* the Introduction section), which induces a diminution in olive fly infestation, and the presence of the bioactive ingredient within the clay, which leads to a more marked interference action.

During the 2019 campaign, there was a medium-high level of infestation in the olive groves. All treated trees showed a lower infestation percentage than the control ones in all observations (T1, T2 and T3) (Fig. 12). Zeo achieved a very good performance in terms of infestation abatement, much more than

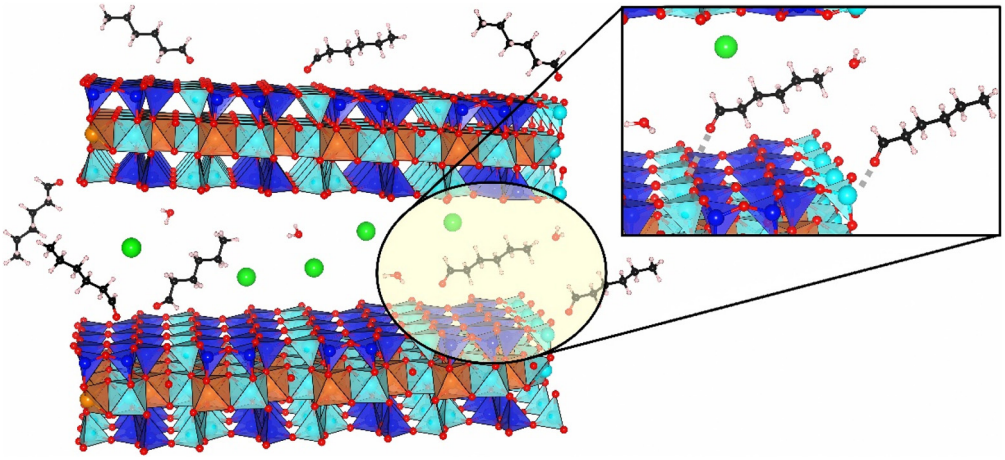

Fig. 10 A schematic depiction of the possible interaction between the clay and the bioactive aldehydes.

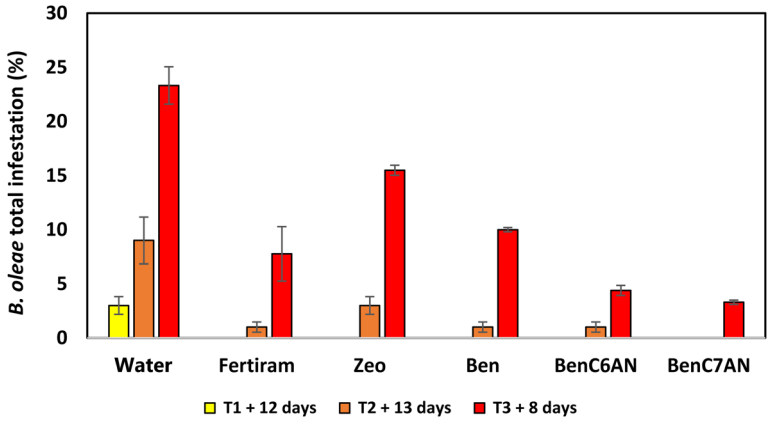

Fig. 11 Percentage of *B. oleae* total infestation on olive fruits recorded after T1 (yellow), T2 (orange) and T3 (red) treatments with various formulations in aqueous suspension (3.1 wt% in drinkable water for test solids). Commercial Fertiram™ formulation as a control. Visual monitoring on 100 olives per tree and sampling of 30 olives for detailed observation in the lab; 2018 trial; Podere Forte farm (Castiglione d'Orcia, Siena, Italy).

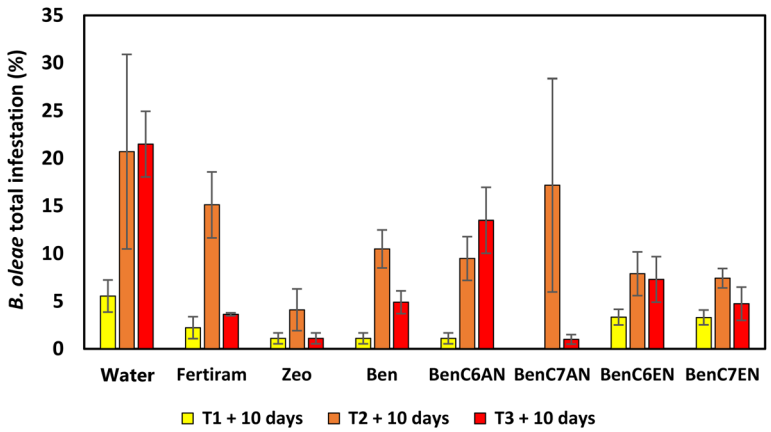

Fig. 12 Percentage of *B. oleae* total infestation on olive fruits recorded after T1 (yellow), T2 (orange) and T3 (red) treatments with various formulations in aqueous suspension (3.1 wt% in drinkable water for test solids). Commercial Fertiram™ formulation as a control. Visual monitoring on 100 olives per tree and sampling of 30 olives for detailed observation in the lab; 2019 trial; Marchesi Mazzei farm (Fonterutoli, Siena, Italy).

in the trials of the previous year (*cf.* Fig. 11). In general, the good effectiveness of aldehyde-containing clay materials was confirmed in this year's trial too and, in particular, excellent results were observed with BenC7AN, which, at the end of the campaign (early October), had a total infestation rate of only 1%. The results for the clays containing unsaturated aldehydes are quite uniform and good as well. Conversely, the result shown after the third treatment with BenC6AN is unexpectedly scarce, at least in this specific trial and under the tested pedological and meteo-climatic conditions. The factors governing the olive fly infestation are indeed multifaceted and a unique explanation for their value is not available at the moment.

Conclusions

The innovative hybrid materials developed within this work rely on montmorillonite-containing bentonite natural clays functionalized with linear aliphatic C_6 or C_7 aldehydes through a cost-effective and technologically simple incipient-wetness deposition method. These organic/inorganic solids synergistically merge two functions: the signalling and deterrent action of the short-chain aldehydic semiochemicals, which interferes with the egg-laying activity of female flies on the olive drupe, and the masking action of the bentonite clay itself, which negatively affects the normal recognition of the olive tree and fruit by adult insects. Thanks to the delicate balance of non-covalent interactions between the aldehyde and the layered solid, the final materials show a fair robustness against weathering and leaching of the active ingredient, but, at the same time, they allow a smooth and constant release of the semiochemical in the surrounding atmosphere. This assures a long-lasting inhibition effect against *B. oleae* fly attacks in open-field trials with promising performance in controlling infestation across two years in two locations with different pedological and meteo-climatic characteristics. The strategy based on the immobilization of bioactive species within the interlayer spaces of the clay allows for the use of lower concentrations of these substances, reducing the unnecessary dispersal of active molecules into the environment. Furthermore, the direct application of bentonite to the entire plant can positively impact the physico-chemical behaviour of the soil near the roots. However, further research is needed to better understand the relationship between these substances and the microflora of olive plants. Such an approach can also be applied to other bioactive species that can be straightforwardly immobilized into clay-based micronized solids to obtain large-scale, sustainable and alternative tools in the control strategy against crop infestation by noxious pests and phytophagous organisms.

Conflicts of interest

There are no conflicts to declare.

Acknowledgements

CNR-SCITEC and CREA-DC acknowledge financial support from the Italian Ministry of Agricultural, Food and Forestry Policies (MIPAAF) through the Project "DIOL – DIfesa da organismi nocivi in OLivicoltura tradizionale e intensiva" (grant prot. no. 23774). The authors also gratefully acknowledge Podere Forte and Azienda Marchesi Mazzei for hosting the open-field tests and Biohelp your Planet and Laviosa Chimica Mineraria for providing free samples of mineral solid materials.

References

1 P. Karanikolas, V. Martinez-Gomez, F. Galli, P. Prosperi, P. A. Hernández, L. Arnalte-Mur, M. Rivera, G. Goussios, L. Fastelli, E. Oikonomopoulou and A. Fonseca, *Global Food Secur.*, 2021, **28**, 100499, DOI: **10.1016/j.gfs.2021.100499**.
2 Z. Zhao, J. R. Carey and Z. Li, *Annu. Rev. Entomol.*, 2024, **69**, 219–237.
3 R. Malheiro, S. Casal, P. Baptista and J. A. Pereira, *Sci. Hortic.*, 2015, **194**, 208–214.
4 L. Medjkouh, A. Tamendjari, S. Keciri, J. Santos, M. A. Nunes and M. B. Oliveira, *Food Funct.*, 2016, **7**, 2780–2788.
5 M. Sinno, A. Bézier, F. Vinale, D. Giron, S. Laudonia, A. P. Garonna and F. Pennacchio, *Pest Manage. Sci.*, 2020, **76**, 3199–3207.
6 J. T. Margaritopoulos, G. Skavdis, N. Kalogiannis, D. Nikou, E. Morou, P. J. Skouras, J. A. Tsitsipis and J. Vontas, *Pest Manage. Sci.*, 2008, **64**(9), 900–908.
7 V. Caleca, A. Belcari and P. Sacchetti, *Protezione delle colture*, 2012, vol. 3, pp. 27–33.
8 M. F. Gonçalves, S. A. P. Santos and L. M. Torres, *Phytoparasitica*, 2012, **40**, 17–28, DOI: **10.1007/s12600-011-0195-z**.
9 D. B. Thomas and R. L. Mangan, *J. Econ. Entomol.*, 2005, **98**(6), 1950–1956.
10 A. Van Scoy, A. Pennell and X. Zhang, *Rev. Environ. Contam. Toxicol.*, 2016, **237**, 53–70.
11 European Food Safety Authority (EFSA), *EFSA J.*, 2016, **14**(4), 4461.
12 E. G. Kakani, N. E. Zygouridis, K. T. Tsoumani, N. Seraphides, F. G. Zalom and K. D. Mathiopoulos, *Pest Manage. Sci.*, 2010, **66**, 447–453.
13 A. Kampouraki, M. Stavrakaki, A. Karataraki, G. Katsikogiannis, E. Pitika, K. Varikou, *et al.*, *J. Pest Sci.*, 2018, **91**, 1429–1439.
14 E. G. Kakani and K. D. Mathiopoulos, *J. Appl. Entomol.*, 2008, **132**, 762–771.
15 A. F. Spanedda and A. Terrosi, *Acta Hortic.*, 2002, **586**, 849–852, DOI: **10.17660/ActaHortic.2002.586.184**.
16 P. J. Skouras, J. T. Margaritopoulos, N. A. Seraphides, I. M. Ioannides and E. G. Kakani, *Pest Manage. Sci.*, 2007, **63**, 42–48.
17 A. F. Spanedda and A. Terrosi, *Acta Hortic.*, 2002, **586**, 853–856, DOI: **10.17660/ActaHortic.2002.586.185**.

18 ISMEA supply balance sheet, https://www.ismeamercati.it/flex/cm/pages/ServeBLOB.php/L/IT/IDPagina/4542 (accessed March 2024).
19 European Commission, Commission Regulation (EU) No 1090/2019 of 26 June 2019, Off. J. Eur. Union, 2019, 173, 39–41.
20 D. M. Glenn and G. J. Puterka, *Hortic. Rev.*, 2005, **31**, 1–44.
21 C. A. D. Silva and F. S. Ramalho, *J. Pest Sci.*, 2013, **86**, 563–569.
22 R. R. Sharma, S. Vijay Rakesh Reddy and S. C. Datta, *Appl. Clay Sci.*, 2016, **116–117**, 54–68.
23 S. E. Abd El-Aziz, *J. Appl. Sci. Res.*, 2013, **9**, 3141–3145.
24 S. C. Albacete, D. M. Amalin, T. M. Carvajal and J. C. Wise, *Front. Agron.*, 2023, **5**, 1213131, DOI: 10.3389/fagro.2023.1213131.
25 C. De Smedt, E. Someus and P. Spanoghe, *Pest Manage. Sci.*, 2015, **71**(10), 1355–1367.
26 C. A. D. Silva and F. S. Ramalho, *J. Pest Sci.*, 2013, **86**, 563–569, DOI: 10.1007/s10340-013-0483-0.
27 D. W. Breck, *Zeolite molecular sieves*, Wiley, New York, 1974.
28 G. Saour and H. Makee, *J. Appl. Entomol.*, 2004, **128**, 28–31.
29 A. Rotondi, L. Morrone, O. Facini, B. Faccini, G. Ferretti and M. Coltorti, *Foods*, 2021, **10**, 1291.
30 M. Rehakova, S. Cuvanova, M. Dzivak, J. Rimar and Z. Gavalova, *Curr. Opin. Solid State Mater. Sci.*, 2004, **8**, 397–404.
31 E. Daher, N. Cinosi, E. Chierici, G. Rondoni, F. Famiani and E. Conti, *Insects*, 2022, **13**, 213.
32 E. Gargani, S. Simoni, C. Benvenuti, R. Frosinini, G. Barzanti, P. Roversi, A. Caselli and M. Guidotti, *Redia*, 2018, **101**, 201–205.
33 G. S. Germinara, A. De Cristofaro and G. Rotundo, *Atti Accadademia Nazionale Italiana di Entomologia*, 2016, 67–71, ISBN 978-88-96493-11-3.
34 R. Malheiro, S. Casal, P. Baptista and J. A. Pereira, *Trends Food Sci. Technol.*, 2015, **44**, 226–242.
35 D. Marchini, R. Petacchi and S. Marchi, *Bull. Insectology*, 2017, **70**, 121–128.
36 R. Malheiro, S. Casal, S. C. Cunha, P. Baptista and J. A. Pereira, *PLoS One*, 2015, **10**(5), e0125070, DOI: 10.1371/journal.pone.0125070.
37 R. Malheiro, A. Ortiz, S. Casal, P. Baptista and J. A. Pereira, *Ind. Crops Prod.*, 2015, **77**, 81–88.
38 S. Marchesi, G. Paul, M. Guidotti, S. Econdi, C. Bisio and F. Carniato, *Inorganics*, 2022, **10**, 159.
39 D. Costenaro, G. Gatti, F. Carniato, G. Paul, C. Bisio and L. Marchese, *Microporous Mesoporous Mater.*, 2012, **162**, 159–167.
40 G. Paul, C. Bisio, I. Braschi, M. Cossi, G. Gatti, E. Gianotti and L. Marchese, *Chem. Soc. Rev.*, 2018, **47**, 5684–5739.
41 M. Gibson, B. C. Percival, M. Edga and M. Grootveld, *Foods*, 2023, **12**(6), 1254.
42 G. Dugo, A. Rotondo, D. Mallamace, N. Cicero, A. Salvo, E. Rotondo and C. Corsaro, *Phys. A*, 2015, **420**(15), 258–264.
43 G. Paul, G. E. Musso, E. Bottinelli, M. Cossi, L. Marchese and G. Berlier, *ChemPhysChem*, 2017, **18**, 839–849.
44 V. Sacchetto, G. Gatti, G. Paul, I. Braschi, G. Berlier, M. Cossi, L. Marchese, R. Bagatin and C. Bisio, *Phys. Chem. Chem. Phys.*, 2013, **15**(32), 13275–13287.
45 M. O. J. Azzam, S. I. Al-Gharabli and M. S. Al Harahsheh, *Desalin. Water Treat.*, 2015, **53**, 627–636.
46 C. Takahashi, T. Shirai, Y. Hayashi and M. Fuji, *Solid State Ionics*, 2013, **241**, 53–61.
47 C. M. Ouellet-Plamondon, J. Stasiak and A. Al-Tabbaa, *Colloids Surf., A*, 2014, **444**, 330–337.
48 F. Carniato, C. Bisio, C. Evangelisti, R. Psaro, V. Dal Santo, D. Costenaro, L. Marchese and M. Guidotti, *Dalton Trans.*, 2018, **47**, 2939–2948.
49 G. A. Ikhtiyarova, A. S. Ozcan, O. Gok and A. Ozcan, *Clay Miner.*, 2012, **47**, 31–44.
50 V. Hlavatý and V.Š Fajnor, *J. Therm. Anal. Calorim.*, 2002, **67**, 113–118.